

EXPLORING TERRESTRIAL PLANET FORMATION IN THE TW HYDRAE ASSOCIATION

FRANK J. LOW AND PAUL S. SMITH

Steward Observatory, The University of Arizona, Tucson, AZ 85721; flow@as.arizona.edu, psmith@as.arizona.edu

MICHAEL WERNER AND CHRISTINE CHEN^{1,2}

Jet Propulsion Laboratory, 4800 Oak Grove Dr., Pasadena, CA 91109; mww@ipac.caltech.edu

VANESSA KRAUSE

Division of Physics, Mathematics, and Astronomy, California Institute of Technology, MS 103-33, Pasadena, CA 91125; krause@caltech.edu

MICHAEL JURA

Department of Physics and Astronomy, University of California, Los Angeles, Los Angeles, CA 90095; jura@clotho.astro.ucla.edu

DEAN C. HINES

Space Science Institute, 3100 Marine Street, Suite A353, Boulder, CO 80303

To Appear in The Astrophysical Journal

ABSTRACT

Spitzer Space Telescope infrared measurements are presented for 24 members of the TW Hydrael association (TWA). High signal-to-noise 24 μm photometry is presented for all of these stars, including 20 stars that were not detected by *IRAS*. Among these 20 stars, only a single object, TWA 7, shows excess emission at 24 μm and at the level of only 40% above the star's photosphere. TWA 7 also exhibits a strong 70 μm excess that is a factor of 40 brighter than the stellar photosphere at this wavelength. At 70 μm , an excess of similar magnitude is detected for TWA 13, though no 24 μm excess was detected for this binary. For the 18 stars that failed to show measurable IR excesses, the sensitivity of the current 70 μm observations does not rule out substantial cool excesses at levels 10–40 \times above their stellar continua. Measurements of two T Tauri stars, TW Hya and Hen 6-300, confirm that their spectacular IR spectral energy distributions (SEDs) do not turn over even by 160 μm , consistent with the expectation for their active accretion disks. In contrast, the *Spitzer* data for the luminous planetary debris systems in the TWA, HD 98800B and HR 4796A, are consistent with single-temperature blackbody SEDs and agree with previous IR, sub-millimeter, and millimeter measurements. The major new result of this study is the dramatic bimodal distribution found for the association in the form of excess emission at a wavelength of 24 μm , indicating negligible amounts of warm ($\gtrsim 100$ K) dust and debris around 20 of 24 stars in this group of very young stars. This bimodal distribution is especially striking given that the four stars in the association with strong IR excesses are $\gtrsim 100\times$ brighter at 24 μm than their photospheres. Clearly, two terrestrial planetary systems, HD 98800B and HR 4796A, exist in some form. In addition, there are at least two active accreting objects, TW Hya and Hen 6-300, that may still be forming planetesimals. The remaining stars may possess significant amounts of cold dust, as in TWA 7 and TWA 13, that have yet to be found.

Subject headings: infrared: stars—circumstellar matter—planetary systems: formation

1. INTRODUCTION

While calibrating the *Infrared Astronomical Satellite* (*IRAS*) Aumann et al. (1984) and Gillett (1986) discovered large far-infrared excesses around four nearby stars: Vega, Fomalhaut, β Pictoris, and ϵ Eridani. Release of the *IRAS* Point Source Catalog led investigators to many other young, nearby dwarf stars displaying excess emission at mid- and far-IR wavelengths (e.g., Walker & Wolstencroft 1988; de la Reza et al. 1989; Gregorio-Hetem et al. 1992; Mannings & Barlow 1998; Zuckerman & Becklin 1993). As a result, numerous investigations of these objects from the ground have added critical insights concerning circumstellar material (e.g., Jayawardhana et al. 1998; Koerner et al. 1998; Kenyon & Bromley 2002, 2004). The *Hubble*

Space Telescope (*HST*) and the *Infrared Space Observatory* (*ISO*) (Habing et al. 2001; Spangler et al. 2001; Meyer & Beckwith 2000, and references therein) have also given us key insights into specific objects, including images taken in the near-IR showing scattered light from thin disks of dust that are shown to absorb starlight and re-emit at much longer wavelengths (e.g., Schneider et al. 1999). Thus, in the last 20 years a body of observations, measurements, analysis and theory have accumulated that leave no doubt about the reality of terrestrial planetary material around young stars. Now, investigations of planetary debris systems (PDSs) are underway with the new tools provided by the *Spitzer Space Telescope* (Werner et al. 2004).

We have initiated a program using *Spitzer* to explore a unique and varied sample of late-type stars that are nearby, \sim 40–100 pc, and show one or more indications of young age. Our total sample of over 120 stars has been

¹ National Research Council Resident Research Associate.

² Current address: National Optical Astronomy Observatories, Tucson, AZ 85719; chen@noao.edu

prioritized into three groups: (1) the first 19 stellar systems identified by common space motion as members of the TW Hydreae association (TWA; Kastner et al. 1997; Webb et al. 1999), (2) ~ 60 stars that show significant lithium absorption indicating young ages, noting that all of the TWA systems easily meet this requirement and therefore overlap this sample, (3) a group of ~ 60 stars with less certain ages based on either detection of X-rays or $\text{H}\alpha$ in emission.

A combination of special circumstances dictate that we start our exploration with the TW Hydreae association. First, the estimated age of the association ranges from 8–10 million years (Myr) and the ages of these stars are essentially equal (Stauffer, Hartmann, & Barrado y Navascués 1995). Second, the TWA members are among the closest young stars available. Third, most association members lie in excellent, low-background regions of the sky for far-IR observations. *IRAS* has already shown that four of the brightest IR excesses known are found in the TWA. Additional important factors are that five of the TWA stars have *Hipparcos* distances averaging around 50 pc, their spectral types range from A0V to M5V with most objects being of M or late K spectral type, and almost all members show signs of T Tauri activity. TW Hydreae itself has been classified as a classic T Tauri system despite its apparent isolation (Herbig, G. H. 1978; Rucinski & Krautter 1983). In contrast, and within the same association, the brightest and most dramatic PDS, HD 98800, shows no evidence for current accretion of primordial material onto the star and has served as the most direct proof of ongoing terrestrial planet formation (e.g., Low, Hines, & Schneider 1999).

2. OBSERVATIONS

Observations of 24 members of the TW Hydreae association were made using *Spitzer*. These include 14 single stars and binaries that are unresolved at 24 μm and five binary systems at least partially resolved by *Spitzer* at 24 μm . The Multi-band Imaging Photometer for *Spitzer* (MIPS; Rieke et al. 2004) provided measurements or upper limits of the flux densities (F_ν) at 24 μm and 70 μm for the entire sample. MIPS 160 μm photometry was also obtained for the four IR-excess systems discovered by *IRAS* (i.e., TW Hya, Hen 3-600, HD 98800B, and HR 4796A). The observations were made between 2004 January 30 and June 21, with each target observed in all of the intended wavelength bands during a single visit by *Spitzer*. Table 1 lists the stars in the association observed with MIPS along with basic data from previous measurements. Six other systems have been identified as members of the TWA (see e.g., Song et al. 2003; Webb 2000a) since the final planning of the *Spitzer*/MIPS observations, but were not included in the target list because of time limitations.

The MIPS data are reduced using the data analysis tool (DAT) of the MIPS instrument team (Gordon et al. 2005). The images are corrected for distortion, registered, and mosaicked to compensate for the movements of the spacecraft and cryogenic scan mirror mechanism (CSMM) within MIPS that are employed to produce a series of spatially dithered images on the three detector arrays. Aperture photometry is then performed on the calibrated, mosaicked images. Table 2 summarizes the

MIPS bandpasses, aperture photometry parameters, and the calibration factors adopted for the data reduction. The data have been color corrected using the relevant tables in the *Spitzer* Observer's Manual.

The 24 μm data were collected using the standard MIPS point source observing template that obtains 14 images of the target at various standard locations on the 128 \times 128-pixel Si:As detector array during each cycle of the template. Either 3 s or 10 s integration times and 1–4 complete template cycles were used to ensure high signal-to-noise ratio (S/N) measurements of the targets. Total observation times were estimated for each target so that a S/N > 10 measurement was achieved at the expected 24 μm flux level of the star's photosphere, and all stars were detected to at least this S/N. Indeed, the median S/N is ~ 160 , though the internal photometric calibration is estimated to be 1–2% in this bandpass (e.g., Rieke et al. 2005).

For the aperture photometry of the 24 μm data, an aperture 15'' in radius (r) was typically used along with a sky annulus centered on the aperture and having an inner radius of $\sim 63''$ and width of 25''. The large sky annulus was chosen to avoid as much flux as reasonable from the *Spitzer* plus MIPS point spread function (PSF) of the target. A larger aperture ($\sim 37.5''$ radius) was used for four binary TWA systems that are at least partially resolved at 24 μm (TWA 8, 9, 13, and 15). The relative brightnesses of individual components of the binaries were estimated by comparing the fluxes measured in $r = 2.5''$ apertures centered on the components. For TWA 9 and 13, a third source of 24 μm flux fell within the large photometric apertures. The flux from these sources were subtracted and are not included in the values for F_ν at 24 μm .

Only HD 98800 was bright enough that the core of the PSF saturated even in the minimum observation time allowed at 24 μm . In this case, the flux in the saturated core was estimated by measuring the flux in the wings of the PSF. This was done for the entire sample as well. The exercise on the non-saturated stars showed that the 24 μm flux in the saturated portion of the PSF for HD 98800 could be recovered to within 5%. After correcting for the saturated core, the 24 μm flux density was measured for HD 98800 in the usual manner.

Observations, data reduction, and aperture photometry for the 70 μm data are similar to those at 24 μm . However, the pixel scale of the 70 μm wide-field optical train ($\sim 10''$ pixel $^{-1}$) dictates that none of the binaries in the TWA can be resolved except for TWA 19. Therefore, we have used a uniform photometry aperture (3-pixel radius) and sky annulus (radius = 4–6 pixels) for the stars observed in the 70 μm wide-field mode. The chosen photometry aperture is very large compared to the $\lesssim 1''$ pointing accuracy of the telescope, eliminating the ambiguity in both the target position on the array and the determination of flux density upper limits for undetected sources.

TW Hya, HD 98800, and HR 4796A were observed in the 70 μm narrow-field mode to prevent saturation by these bright IR sources as this optical train halves the pixel scale. For these observations, an $r = 5.67''$ aperture was chosen. Instead of an annulus centered on the target to estimate the sky contribution within the photometric aperture, rectangular regions on either side of the target

were utilized because of the narrow, 16-pixel width of the usable portion of the detector array.

Because of the degraded sensitivity and higher instrumental noise of the $70\text{ }\mu\text{m}$ Ge:Ga detector array relative to pre-launch estimates, it was not practical to obtain measurements accurate enough to detect objects at the expected levels of the TWA photospheres. As a result, the $70\text{ }\mu\text{m}$ observations were tailored to detect excesses at flux levels $\gtrsim 10\times$ the expected $70\text{ }\mu\text{m}$ photospheric flux density with a reasonably high degree of confidence ($>3\text{--}4\sigma$). Unfortunately, most of the TWA observations occurred before the bias level for the $70\text{ }\mu\text{m}$ detector was reduced. During the period before the bias change, the overall noise in the detector was greater and there were more pronounced changes seen in background levels across array modules. Because of these instrumental effects, a conservative criterion of 5σ above background was adopted for a detection at $70\text{ }\mu\text{m}$.

All four targets observed at $160\text{ }\mu\text{m}$ were detected at a S/N ranging from $\sim 6\text{--}160$ using the standard MIPS photometry observing template. In all cases, an aperture of $r = 64''$ was used for the photometry. The sky contribution within the photometric aperture was estimated using rectangular regions on either side of the target. As with the $24\text{ }\mu\text{m}$ and $70\text{ }\mu\text{m}$ data, the $160\text{ }\mu\text{m}$ photometry is corrected for the loss in flux caused by the use of apertures of finite size not encompassing the total flux from the PSF. The multiplicative aperture corrections to a hypothetical aperture of infinite extent are listed in Table 2.

The $160\text{ }\mu\text{m}$ data were also corrected for the blue filter leak discovered in this bandpass after the launch of *Spitzer*. This leak allows light at $\sim 2\text{ }\mu\text{m}$ in wavelength to reach the detector which is sensitive to near-IR radiation. Tests made during flight have shown that the contaminating flux is about $15\times$ the flux received from a star's photosphere at $160\text{ }\mu\text{m}$ assuming a Rayleigh-Jeans law between the near and far-IR. In all four cases in the TWA where $160\text{ }\mu\text{m}$ measurements were made, the expected photospheric $160\text{ }\mu\text{m}$ flux density is $\ll 1\%$ of the measured signal. Given the bright far-IR excesses of these stars, the filter leak corrections are small.

In addition to broad-band photometry, observations of TW Hya and HD 98800 were made using MIPS in its SED mode. These observations were made on JD = 2453395, roughly a year after the MIPS photometry of TW Hya was obtained and about seven months after the photometry of HD 98800. In this observing mode, the CSMM brings light from the telescope to a reflective diffraction grating that also performs the functions of a slit and collimator. The collimated, dispersed light is then focused onto the $70\text{ }\mu\text{m}$ detector array. The result is a very low-resolution ($R = \lambda/\Delta\lambda \sim 15\text{--}25$) first-order spectrum covering a wavelength range of $52\text{--}97\text{ }\mu\text{m}$. The slit/grating has a width of two pixels ($\sim 20''$) and the dispersion is $1.7\text{ }\mu\text{m pixel}^{-1}$. An unusable portion of the $70\text{ }\mu\text{m}$ array restricts the slit length to $\sim 2.7'$. Also, a dead 4×8 -pixel readout at one end of the slit further reduces the effective length of the slit where the full spectral range can be sampled.

Observations in SED mode involve chopping the CSMM between the target and a region $1\text{--}3'$ away to sample the background, and using small spacecraft moves to dither the target between two positions along the slit.

Data reduction is again handled by the DAT in essentially the same manner as for $70\text{ }\mu\text{m}$ broad-band imaging. The result is co-added “on-” and “off-target” images. After the background image has been subtracted from the target, the spectrum is extracted using an extraction aperture of set width (8 pixels). Flux calibration of the TW Hya and HD 98800 spectra was accomplished using a MIPS SED-mode observation of α Boo made on JD = 2453196. The $50\text{--}100\text{ }\mu\text{m}$ continuum of α Boo is assumed to be $\propto \lambda^{-2}$ and $F_\nu = 14.7\text{ Jy}$ at the effective wavelength of the $70\text{ }\mu\text{m}$ filter bandpass. The observations and spectral extractions of α Boo and the two TWA systems were identical and the same DAT calibration files were used for every target.

3. RESULTS

Table 3 summarizes the MIPS photometric results for the TWA. Several stars in the association are known optical variables and we give the epoch of the start of the observations in the second column of the table. The $24\text{ }\mu\text{m}$, $70\text{ }\mu\text{m}$, and $160\text{ }\mu\text{m}$ flux densities are given in units of milli-Janskys (mJy; where $1\text{ mJy} = 10^{-26}\text{ erg cm}^{-2}\text{ s}^{-1}\text{ Hz}^{-1}$). Uncertainties in the flux densities are the square root of the quadratic sum of the measurement and calibration uncertainties, noting that most relative uncertainties are much lower. Also listed in Table 3 is the S/N of the detections in each MIPS band. Although some of the S/N values are extremely high, the uncertainties quoted for the photometry in all three bandpasses are dominated by uncertainties in the absolute flux calibration of the instrument. These are estimated to be $\sim 10\%$ for the $24\text{ }\mu\text{m}$ band and $\sim 20\%$ for the $70\text{ }\mu\text{m}$ and $160\text{ }\mu\text{m}$ bandpasses. Upper limits assigned in Table 3 to non-detections at $70\text{ }\mu\text{m}$ are at the level of 3σ over the noise of the background.

Our primary goal for this observational program is to detect and measure IR excesses in the TWA. This requires that good estimates of F_ν be made for the TWA stellar photospheres at the effective wavelengths of the MIPS bandpasses. For all of stars in the sample, stellar photospheres were derived using a grid of Kurucz (Kurucz 1979) and “NextGen” (Hauschildt, Allard, & Baron 1999) photospheric models and fitting available optical photometry combined with near-IR flux densities compiled from the Two-Micron All Sky Survey (2MASS) Point Source Catalog. Temperature is a free parameter in the fitting, but in all cases solar metallicity and $\log g = 4.5$ are assumed. The NextGen models are known to yield better fits to late-type main sequence stars than Kurucz models, and were used for all TWA members except for HR 4796A and TWA 19A, which have much higher effective temperatures than the rest of the sample. The best-fitting model temperatures (T_*) of the TWA are listed in Table 1.

3.1. $24\text{ }\mu\text{m}$ Excesses

Comparison of the $24\text{ }\mu\text{m}$ data for the TWA with the 2MASS K_s -band flux densities of these stars shows that the association can essentially be divided into two populations. Figure 1 plots the 24 -to- $2.17\text{ }\mu\text{m}$ flux density ratio against the flux density in the K_s -band. In all cases, the 2MASS photometry is consistent with the stellar photospheres emitting the near-IR light. The four stars with IR excesses discovered by *IRAS* are about a factor of 100

brighter at 24 μm relative to K_s than the other stars in the sample. In fact, for the stars with flux ratios <0.02 , the data are consistent with the 24 μm flux being solely from the photosphere. As a guide, a dashed line in Figure 1 marks the limit of $F(24 \mu\text{m})/F_{K_s}$ if both bandpasses fall within the Rayleigh-Jeans regime of the stellar continuum. Since the TWA members are typically spectral type K and M, the K_s band falls close to the emission peak of the photosphere. As a result, the stars typically lie above the Rayleigh-Jeans limit in Figure 1.

Figure 2 further explores the empirical relation between the 24 μm flux density with the near-IR. The stars with previously known IR excesses or $T_* > 4500$ K are omitted from Figure 2, and the flux ratio shown in Figure 1 is now plotted against the temperature of the model stellar photosphere. The majority of the 19 stars plotted form a locus that is offset from the $F(24 \mu\text{m})/F_{K_s}$ ratios expected from blackbodies. Spectra derived from the NextGen models generally give a good approximation to the observed flux ratios, although the TWA members have not reached the main sequence. The unweighted average flux ratio $\langle F(24 \mu\text{m})/F_{K_s} \rangle = 0.015$ with an RMS of only 0.004. The concentration of the points close to the expected values from the NextGen models in Figure 2 suggests that we are seeing no IR excess at 24 μm for most of these late-type, young stars. The MIPS photometry is consistent with the 24 μm flux emanating from the photosphere for most of the members of the TWA. One example is TWA 6, where the MIPS 24 μm measurement supports the contention by Uchida et al. (2004) that the 5–20 μm spectrum of this star taken with *Spitzer* and the Infrared Spectrograph (IRS; Houck et al. 2004) is indeed the spectrum of the photosphere.

Although the NextGen models yield a much better brightness estimate of the photosphere at 24 μm than blackbodies in this temperature range, Figure 2 shows that the flux ratio is possibly more dependent on the model temperature than is actually observed. Note, TWA 12, 13B, and 17 fall well below the NextGen curve. These deviations and the intrinsic scatter of the data are intriguing, but the limited number of objects in the sample complicate a detailed investigation of their possible causes, especially considering that only temperature was varied in constructing the models and that the TWA stars are younger than the nominal zero-age main sequence stars described by the NextGen models. In the case of TWA 17, the 24 μm flux density is measured to be only 1.5 ± 0.2 mJy and the source is detected at a $S/N = 13$ with MIPS. Therefore, we do not confirm the possible excess at 12 and 18 μm reported from ground-based observations by Weinberger et al. (2004).

The measurement of $F(24 \mu\text{m})/F_{K_s}$ for TWA 7 suggests that it possesses a 24 μm excess that contributes $\sim 40\%$ to the total brightness of this system at this wavelength. Except for the four *IRAS* detections, TWA 7 has a higher flux ratio in Figures 1 and 2 than all of the other TWA members. The next highest ratio belongs to TWA 9B, but its deviation from the expected flux of the photosphere is less than half of that shown by TWA 7, and is no larger than the flux deficits at 24 μm measured for TWA 12, 13B, and 17. Since the 2MASS and MIPS measurements are not simultaneous, an alternate explanation for the apparent IR excess in TWA 7 could be the variability of the star which is not uncommon for

T Tauri stars, although there are no published data suggesting that this star is variable. Also, the clustering of most measurements around $\langle F(24 \mu\text{m})/F_{K_s} \rangle$ is a clear demonstration that most stars in the TWA do not, in fact, exhibit significant variability.

3.2. 70 μm Excesses

Regardless of the strength of a possible 24 μm excess in the observed continuum of TWA 7, this object is detected at 70 μm at a flux level $\sim 40\times$ brighter than the photospheric emission estimated for the star at this wavelength. Figure 3 presents the ratio between the observed and predicted 70 μm flux densities. Only six of the 20 systems (TWA 19 is resolvable at 70 μm) are detected with MIPS at 70 μm . TWA 13 joins TWA 7 and the four *IRAS* sources in having a detected 70 μm excess. TWA 13 cannot be resolved with *Spitzer* at 70 μm , so it is unknown which of the two components produces the excess, or if both components of the binary contribute to the observed flux.

Figure 3 shows the same basic division in the TWA sample as is found at 24 μm . The 70 μm excesses for TWA 7 and 13 are $\gtrsim 10\times$ fainter than the other detections. One-sigma upper limits are also shown in Figure 3 for the remainder of the sample. As discussed in §2, the sensitivity limits of the 70 μm array render detection of the photospheres of the TWA sample impractical. Excesses similar to those of TWA 7 and 13 cannot be ruled out for many members of the association, and it is clear from the data that it is not necessary for an object to show an excess at 24 μm to find one at 70 μm . For instance, there is no hint from the 24 μm measurement of TWA 13 of an excess at longer wavelengths. There are three stars where a 70 μm excess at $> 10\times$ the flux density of the photosphere can be ruled out at the 3σ confidence level: TWA 2, 5A, and 8A. Therefore, the minimum range in strength for 70 μm excesses in the TWA is greater than a factor of 300.

3.3. Spectral Energy Distributions

The SEDs of the six systems in the TWA with confirmed IR excesses are shown in Figure 4. It is readily apparent that this small sample of young stars exhibits a rich variety of IR properties. The T Tauri stars TW Hya and Hen 3-600 show no hint of their SEDs turning over even out to 160 μm . In fact, the MIPS 160 μm measurement for TW Hya reveals that the spectrum of the presumed optically thick accretion disk continues to rise into the infrared. Similar to TW Hya, the MIPS data for Hen 3-600 are consistent with the earlier *IRAS* results and show that the 70 and 160 μm flux densities are roughly equivalent.

In contrast, HD 98800A and B do not show the extreme activity associated with T Tauri stars. However, HD 98800B generates a huge IR excess that is well fit by a single blackbody with $T = 160$ –170 K (Low, Hines, & Schneider 1999; Hines et al. 2004), whereas component A lacks an easily measured excess even though the total luminosities of the two companions are virtually identical. The MIPS photometry is consistent with earlier results. Likewise, the IR excess of HR 4796A produces an IR SED that can be fit by a single blackbody, but it is significantly cooler than found for HD 98800B ($T = 110$ K; Jura et al. 1993). With the

addition of the *Spitzer* observations, we fit this excess with a $T = 108$ K blackbody. Given that HR 4796A is an A0V star, it is not surprising that it has an IR excess because of the finding that younger A stars have a higher probability of possessing a 24 μm excess and having stronger thermal excess emission than older A stars (Rieke et al. 2005). It is of note that HR 4796A has by far (by $\sim 10\times$) the largest ratio of 24 μm excess emission-to-photospheric emission of the 265 A and B stars examined by Rieke et al. (2005).

Figure 5 presents the MIPS SED-mode observations of TW Hya and HD 98800B. These low-resolution spectra do not show any spectral features of high equivalent width in either object. Arcturus was used to calibrate the spectra and they are consistent with the 70 μm flux densities derived from the photometry. The IR spectral slopes of TW Hya and HD 98800B are quite different, with the continuum of TW Hya being much redder than that of HD 98800B. A power-law having a spectral index, α , where $F_\nu \propto \nu^\alpha$, is adequate to describe these data. For TW Hya, $\alpha = -0.33 \pm 0.04$, and is consistent with the finding that the 160 μm flux density is higher than the 70 μm measurement. The slope of a single power-law fit to the continuum of HD 98800B between 52 and 97 μm yields $\alpha = 1.12 \pm 0.04$. The blackbody fit with $T_{BB} = 160$ K to the PDS of HD 98800B is also shown in Figure 5, and its slope within this spectral region is in good agreement with the SED-mode data.

3.4. PDS Luminosity and Mass

Our primary reason for calculating the stellar and IR excess luminosity is to measure the fractional luminosities of those stars that show direct evidence of PDS formation and to provide well defined upper limits for those stars that fail to show an excess. Table 4 lists the stellar luminosity, L_* , derived by numerical integration, and the fractional luminosity, L_{IR}/L_* , where L_{IR} is the luminosity of the infrared excess that is the result of numerically integrating the flux density in excess of the predicted level of the photosphere. Direct measurements of the distance to TWA members are limited to only five systems (Table 1). We have assigned a distance of 55 pc, the distance corresponding to the unweighted average of the parallaxes measured by *Hipparcos* excluding TWA 19, to the other stars in the sample. In general, L_* is higher than expected for the TWA given their spectral types because these young, rapidly evolving stars have higher luminosities, lower temperatures, and larger radii than when they reach the main sequence.

Conservative upper limits for L_{IR}/L_* have been assigned to objects listed in Table 4 that show no evidence for a 24 μm excess by assuming that the 1σ upper limits estimated for the 70 μm flux densities represent the brightness of a possible IR excess plus photosphere at this wavelength. It is also assumed that any possible IR excess is well approximated by a blackbody with temperature, T_{PDS} . The upper limit on the temperature of a possible cold PDS is given in Table 4 and is set so that T_{PDS} and the assumed value for $F(70 \mu\text{m})$ raise $F(24 \mu\text{m})$ by no more than 10%; the adopted uncertainty in the absolute flux calibration of the MIPS measurements at 24 μm . These upper limits on temperature do not preclude small amounts of warmer dust within systems that are still consistent with the 24 μm mea-

surements, but they do constrain the properties of circumstellar material able to produce substantial excesses at 70 μm and be undetected by *Spitzer*.

The mass of circumstellar dust responsible for the luminosity of IR excesses observed in the TWA, or that could produce the upper limits found for T_{PDS} and L_{IR}/L_* , can be deduced following the inferences of Jura et al. (1995) and Chen & Jura (2001). That is, the minimum mass in dust can be estimated by

$$M_d \geq (16/3)\pi(L_{IR}/L_*)\rho R_{PDS}^2 \langle a \rangle$$

(Jura et al. 1995), where $\langle a \rangle$ is the average radius of a dust grain, R_{PDS} is the minimum distance from the star where the grains are in radiative equilibrium, and ρ is the mass density of the grains. The equation above assumes that the dust is radiating from a thin shell at a distance R_{PDS} from the illuminating star and that the debris disk is optically thin. Also, it is assumed that the dust grains are spherical and have cross sections equal to their geometric cross sections. In Table 4, we tabulate M_d using the values for average grain size and density adopted by Chen & Jura (2001) ($\langle a \rangle = 2.8 \mu\text{m}$; $\rho = 2.5 \text{ g cm}^{-3}$). The minimum dust mass responsible for detected IR excesses range from $\sim 10^{25} \text{ g}$ for HR 4796A to $\sim 10^{23} \text{ g}$ for TWA 13. For HD 98800B, the assumption that the debris disk is optically thin is not valid, accounting for the much smaller mass estimate than that determined by Low, Hines, & Schneider (1999).

The mass estimates in Table 4 for the TWA are conservative lower bounds for the total circumstellar dust mass in these systems since the MIPS observations are not sensitive to colder material located further from a star and emission from larger particles. For example, there is evidence for material around TWA 7 colder than the ~ 80 K dust detected by *Spitzer*. Observations at 850 μm by Webb (2000a) detected TWA 7 with $F_\nu \sim 15 \text{ mJy}$. This flux density is about a factor of seven higher than the extrapolation to 850 μm of the ~ 80 K blackbody determined by the 24 and 70 μm excesses. Webb (2000a) and Webb et al. (2000b) interpret the sub-millimeter emission as coming from 20 K dust with grain sizes on the order of a few hundred microns. As a consequence, the mass estimate for the dust disk around TWA 7 derived by the sub-millimeter measurement is $\sim 10^3 \times$ greater than that estimated from the IR excess.

4. DISCUSSION

4.1. Infrared Properties of the TWA

The main result of the *Spitzer*-MIPS observations of the TWA is to show that most stars in the association exhibit no evidence for circumstellar dust and that the 24 μm data place severe limits on the presence of warm ($T \gtrsim 100$ K) dust within these systems. Although the TWA includes four remarkable IR-excess systems, there are no other objects that come close to their 24 μm output relative to the observed near-IR photospheric emission. The bimodal distribution of warm dust in the TWA, identified by Weinberger et al. (2004) at shorter wavelengths, is confirmed at 24 μm for a larger sample of objects (see Figure 1).

The bimodal nature of 70 μm excesses is not as pronounced as at shorter wavelengths, but there is still a gap of about a factor of 10 between the strengths of the 70 μm excess of Hen 3-600 and the *Spitzer* detections of TWA 7

and 13. There is also a range of at least ~ 300 between the brightest and faintest of the $70\ \mu\text{m}$ excesses in the TWA relative to their photospheres at this wavelength. The luminosity of the observed IR excesses range from $\sim 25\%$ (TW Hya and HD 98800B) to $\sim 0.1\%$ (TWA 13) of L_* .

It is difficult to fully characterize the IR excesses of TWA 7 and 13 given that they only begin to appear at $\sim 24\ \mu\text{m}$. In the case of TWA 13, there is also the complicating factor that the system is a binary and the distribution of the material responsible for the excess is unknown. However, calculating a color temperature for the two objects yields similar results: $T_c \sim 60\text{--}80\ \text{K}$. Assuming that the excesses are well fit by blackbodies, both systems have a fractional IR luminosity of $\sim 1\%$ of that measured for HD 98800B; $L_{\text{IR}}/L_* = 2.0 \times 10^{-3}$ and 1.7×10^{-3} , for TWA 7 and 13, respectively. Although the lack of observed excess $24\ \mu\text{m}$ emission constrains the temperatures of possible PDSs for most of the $70\ \mu\text{m}$ non-detections to be $< 100\ \text{K}$, the MIPS observational upper limits cannot rule out IR excesses with fractional luminosity in the range of $10^{-3}\text{--}10^{-4}$. Even at the estimated young age of the association it may already be more likely to detect cooler material, further away from the stars, than warmer material that results in an excess at $24\ \mu\text{m}$ or shorter wavelengths. Clearly, at $70\ \mu\text{m}$ wavelength, large amounts of additional *Spitzer* time will be needed to detect and measure the cool dust and debris around these stars.

The variety of the IR properties in the TWA is remarkable given the assumption that its members have similar ages. At 8–10 Myr after the formation of the TWA, there are still two systems (TW Hya and Hen 3-600) accreting presumably primordial dust and they have enough circumstellar material to reprocess a large fraction (10–30%) of the stellar luminosity into the infrared. Also in the association are two multiple-star systems, HD 98800 and HR 4796, that have a prominent PDS around only one of the stellar components and the debris is relatively warm ($T_{\text{PDS}} = 100\text{--}170\ \text{K}$). TWA 7 shows evidence for a weak $24\ \mu\text{m}$ excess with the detected material being cooler ($T_{\text{PDS}} \sim 80\ \text{K}$) and located in orbits $\gtrsim 7\ \text{AU}$ from the star. The remaining 19 stars, including TWA 7 and 13, have apparently been cleansed to a high degree of dust with $T > 100\ \text{K}$. This variety of properties suggests that dust is swept from regions within several AU (see Table 4) of the star very early in the system’s evolution. The fact that stars in the association show no signature of warm dust while other members exhibit strong T Tauri activity implies that the transition period from the T Tauri stage to the more quiescent state observed for most of the TWA K- and M-type stars, is very short.

An efficient mechanism for the removal of dust is thought to be the formation of planets that sweep up dust and larger debris in the regions that they orbit. Weinberger et al. (2004) suggest that planetary formation was rapidly completed in the TWA at least in the region where terrestrial planets would be expected to form. This led to the rapid disappearance of dust in the inner several AU of these systems, leaving only the stellar photosphere to be detected at wavelengths of $24\ \mu\text{m}$ and shorter. Strong stellar winds during the T Tauri stage and the Poynting-Robertson drag are also mechanisms that can decrease the IR emission from a system by rid-

ding the environment of small dust grains. Of course, in most TWA systems, and within 10 Myr of their formation, dust destruction mechanisms must more than compensate for the dust production mechanism of collisions between larger bodies to clear out the terrestrial planet region. HD 98800B and HR 4796A are likely cases where their debris systems indicate that collisions between bodies are still important and produce dust close enough to the stars to result in large excesses at $24\ \mu\text{m}$.

Nearly all members of the observed sample are X-ray emitters, supporting the assertion that stellar winds in these young, low-mass stars may be an important dust destruction mechanism (see e.g., Hollenbach, Yorke, & Johnstone 2000). We list the X-ray-to-stellar luminosity ratios, L_X/L_* , for TWA stars in the last column of Table 4. The X-ray data are drawn from the *ROSAT* All Sky Survey Catalog and L_X is calculated in the manner described by Sterzik et al. (1999). Chen et al. (2005) find an apparent correlation between IR and X-ray luminosity for their sample of F- and G-type stars with ages spanning 5–20 Myr in the Scorpius-Centaurus OB Association. This possible correlation is in the sense of brighter $24\ \mu\text{m}$ excesses tending to be associated with fainter stars in X-ray flux, and Chen et al. (2005) suggest that the stronger stellar wind implied by the chromospheric activity may help explain the general lack of young systems with $24\ \mu\text{m}$ excesses. Given that only three stars in the TWA sample have confirmed PDSs that produce measurable excesses at $24\ \mu\text{m}$, it is not possible to test the validity of the X-ray–IR flux correlation. However, HD 98800B, HR 4796A, and TWA 7, are all underluminous in X-rays compared to the average observed X-ray emission for the TWA.

4.2. Comparison of the TWA with the Young Solar System

We can compare the *Spitzer* observations of young stars with models for the early Solar System. Following the discussions in Gaidos (1999) and Jura (2004), we assume that the rate of dust production directly scales as the rate of lunar cratering during the Late Heavy Bombardment. The rate of dust production, \dot{M}_{dust} , is given by:

$$\dot{M}_{\text{dust}} = \dot{M}_0 \left(1 + \beta e^{\frac{t_9}{\tau}} \right),$$

where t_9 is the look-back time in $10^9\ \text{yr}$ (Gyr), \dot{M}_0 is the current rate of dust production and β and τ are fitting constants such that $\beta = 1.6 \times 10^{-10}$ and $\tau = 0.144$ (Chyba 1991). In this model, the dust production rate has been approximately constant during the past 3.3 Gyr, but was as high as $\sim 10^4$ the current value when $t_9 = 4.6$. We set $\dot{M}_0 = 3 \times 10^6\ \text{g s}^{-1}$ based on the zodiacal light in the Solar System (Fixsen & Dwek 2002), implying that the early Solar System may have had a dust production rate of $3 \times 10^{10}\ \text{g s}^{-1}$. In a model where this quantity of dust is produced far from the star and then loses angular momentum under the action of the Poynting-Robertson effect, it is straightforward to show (e.g., Gaidos 1999) that the luminosity of the dust, L_ν , is given by the expression:

$$L_\nu = \frac{\dot{M}_{\text{dust}} c^2}{\nu}.$$

For the TWA, young M-type stars would have luminosities at 24 μm of $2 \times 10^{18} \text{ erg s}^{-1} \text{ Hz}^{-1}$ and, for distances of ~ 50 pc, we expect $F_\nu(24 \mu\text{m}) \approx 700 \text{ mJy}$, vastly greater than what is observed. This result suggests the absence of terrestrial planet-forming environments around these stars. However, in M-type stars where the luminosity is relatively low and the stellar wind rate is relatively large, dust grains mainly lose angular momentum by stellar wind drag rather than through Poynting-Robertson drag (see Jura 2004; Plavchan et al. 2005). In this case, and if \dot{M}_{wind} denotes the stellar wind loss rate, then:

$$L_\nu = \frac{\dot{M}_{dust}}{\dot{M}_{wind}} \frac{L_*}{\nu}.$$

Although we do not know \dot{M}_{wind} for young M-type stars, we can extrapolate from their X-ray emission since the winds are likely to be driven by the same hot corona which produces the X-rays. It is plausible that young M-type stars have mass loss rates 10^2 greater than the current Solar wind loss rate of $2 \times 10^{12} \text{ g s}^{-1}$, and we estimate that $\dot{M}_{wind} = 2 \times 10^{14} \text{ g s}^{-1}$. For main sequence early M-type stars, we may adopt $L_* = 0.05L_\odot$. Therefore, we expect that at 24 μm , $L_\nu = 2 \times 10^{15} \text{ erg s}^{-1} \text{ Hz}^{-1}$ and a predicted flux at 50 pc of only $\sim 0.7 \text{ mJy}$. A 24 μm excess this small is beyond the sensitivity of our current measurements, and it is possible that planet forming activity may still be occurring around the young M-type stars in the TWA even though we do not detect an infrared excess.

The TWA gives us an important example of the rapid evolution of the circumstellar material around generally low-mass stars with ages of ~ 10 Myr that is in line with time scales of terrestrial planet formation inferred for our solar system from radiochemistry of meteorites (Yin et al. 2002; Kleine et al. 2002). The diverse IR properties of the association also suggest that the evolutionary processes relevant to planetary formation and accretion disk dispersal may occur at different rates even for stars with similar spectral types. For most of the systems observed, the lack of emission from dust within a few AU of the stars leads to two possible conclusions. Either, (1) the early conditions around pre-main sequence M and late K stars prevent the formation of terrestrial planets in most cases, or that (2) terrestrial planet building has already progressed to the point where the mass is in the form of planetesimals.

This work is based on observations made with the *Spitzer Space Telescope*, which is operated by the Jet Propulsion Laboratory (JPL), California Institute of Technology (CIT), under National Aeronautics and Space Administration (NASA) contract 1407. We thank NASA, JPL, and the *Spitzer* Science Center for support through *Spitzer*, MIPS, and Science Working Group contracts 960785, 959969, and 1256424 to The University of Arizona. We thank M. Blaylock, C. Engelbracht, K. Gordon, K. Misselt, J. Muzerolle, G. Neugebauer, J. Stansberry, K. Stapelfeldt, K. Su, B. Zuckerman, and an anonymous referee for useful comments and discussions. V. Krause acknowledges a Summer Undergraduate Research Fellowship at JPL. This publication makes use of data products from the Two-Micron All Sky Survey,

which is a joint project of the University of Massachusetts and the Infrared Processing and Analysis Center/CIT, funded by NASA and the National Science Foundation.

REFERENCES

Aumann, H. H., et al. 1984, *ApJ*, 278, L23

Beichman, C. A., Neugebauer, G., Habing, H. J., Clegg, P. E., & Chester, T. J. 1988, in *Infrared Astronomical Satellite (IRAS) Catalogs and Atlases*, vol. 1, *Explanatory Supplement*, NASA RP-1190 (Washington, DC: GPO)

Chen, C. H., & Jura, M. 2001, *ApJ*, 560, L171

Chen, C. H., Jura, M., Gordon, K. D., & Blaylock, M. 2005, *ApJ*, 623, 493

Chyba, C. F. 1991, *Icarus*, 92, 217

Cutri, R.M., et al. 2003, *Explanatory Supplement to the 2MASS All Sky Data Release*, <http://www.ipac.caltech.edu/2mass/releases/allsky/doc/explsup.html>

de la Reza, R., Torres, C. A. O., Quast, G., Castilho, B. V., Vieira, G. L. 1989, *ApJ*, 343, L61

Epcstein, N. et al. 1999, *A&A*, 349, 236

European Space Agency 1997, *The Hipparcos and Tycho Catalogues* (Paris: ESA), SP-1200

Fixsen, D. J. & Dwek, E. 2002, *ApJ*, 578, 1009

Gaidos, E. J. 1999, *ApJ*, 510, L131

Gehrzi, R. D., Smith, N., Low, F. J., Krautter, J., Nollenberg, J. G., & Jones, T. J. 1999, *ApJ*, 512, L55

Gillett, F. C. 1986, in *Light on Dark Matter*, ed. F. P. Israel (Dordrecht: D. Reidel), 61

Gordon, K. D., et al. 2005, *PASP*, 117, 503

Gregorio-Hetem, J., Lépine, J. R. D., Quast, G. R., Torres, C. A. O., & de la Reza, R. 1992, *AJ*, 103, 549

Habing, H. J., et al. 2001, *A&A*, 365, 545

Hines, D. C., Low, F. J., Schneider, G., Chandler, C. J., Plait, P., & Smith, P. S. 2004, in *ASP Conference Series*, 324, *Debris Disks and the Formation of Planets: A Symposium in Memory of Fred Gillett*, eds. L. Caroff, L. J. Moon, D. Backman, & E. Praton (San Francisco: ASP), 262

Hollenbach, D. J., Yorke, H. W., & Johnstone D. 2000, in *Protostars and Planets IV*, eds. V. Mannings, A. P. Boss, & S. S. Russell (Tucson: The University of Arizona Press), 401

Hauschildt, P. H., Allard, F., & Baron, E. 1999, *ApJ*, 512, 377

Herbig, G. H. 1978, *Origin of the Solar System* (New York: Wiley-Interscience), 219

Houck, J. R., et al. 2004, *ApJS*, 154, 18

Houk, N. 1982, *Michigan Spectral Survey* (Ann Arbor: University of Michigan Press), 3

Jayawardhana, R., Fisher, S., Hartmann, L., Telesco, C., Piña, R., & Fazio, G. 1998, *ApJ*, 503, L79

Jayawardhana, R., Hartmann, L., Fazio, G., Fisher, R. S., Telesco, C. M., & Piña, R. K. 1999, *ApJ*, 521, L129

Jura, M. 2004, *ApJ*, 603, 729

Jura, M., Ghez, A. M., White, R. J., McCarthy, D. W., Smith, R. C., & Martin, P. G. 1995, *ApJ*, 445, 451

Jura, M., Zuckerman, B., Becklin, E. E., & Smith, R. C. 1993, *ApJ*, 418, L37

Kastner, J. H., Zuckerman, B., Weintraub, D. A., & Forveille, T. 1997, *Science*, 277, 67

Kenyon, S. J., & Bromley, B. C. 2002, *ApJ*, 577, L35

Kenyon, S. J., & Bromley, B. C. 2004, *AJ*, 127, 513

Kleine, T., Münker, C., Mezger, K., & Palme, H. 2002, *Nature*, 418, 952

Koerner, D. W., Ressler, M. E., Werner, M. W., & Backman, D. E. 1998, *ApJ*, 503, L83

Kurucz, R. L. 1979, *ApJS*, 40, 1

Lasker, B. M., Stuch, C. R., McLean, B. J., Russell, J. L., Jenker, H., & Shara, M. 1990, *AJ*, 99, 2019

Low, F. J., Hines, D. C., & Schneider, G. 1999, *ApJ*, 520, L45

Mamajek, E. E., Lawson, W. A., & Feigelson, E. D. 2000, *ApJ*, 544, 356

Mannings, V. i., & Barlow, M. J. 1998, *ApJ*, 497, 330

Meyer, M. R., & Beckwith, S. V. W. 2000, in *ISO Surveys of a Dusty Universe*, eds. D. Lemke, M. Stickel, & K. Wilke (New York: Springer), 341

Monet, D. G. 1999, *USNO A2.0* (CD-ROM)

Perryman, M. A. C., et al. 1997, *A&A*, 323, L49

Platais et al. 1998, *AJ*, 116, 2556

Plavchan, P., Jura, M., & Lipsky, S. 2005, *ApJ*, in press

Prato, L., et al. 2001, *ApJ*, 549, 590

Reid, N. 2003, *MNRAS*, 342, 837

Rieke, G. H., et al. 2005, *ApJ*, 620, 1010

Rieke, G. H., et al. 2004, *ApJS*, 154, 25

Rucinski, S. M., & Krautter, J. 1983, *A&A*, 121, 217

Schnieder, G., et al. 1999, *ApJ*, 513, L127

Soderblom D. R., et al. 1998 *ApJ*, 498, 385

Spangler, C., Sargent, A. I., Silverstone, M. D., Becklin, E. E., & Zuckerman, B. 2001, *ApJ*, 555, 932

Song, I., Zuckerman, B., & Bessel, M. S., 2003, *ApJ*, 599, 342

Stauffer, J. R., Hartmann, L. W., & Barrado y Navascues, D. 1995, *ApJ*, 454, 910

Sterzik, M. F., Alcalá, J. M., Covino, E., & Petr, M. G. 1999, *A&A*, 346, L41

Torres, C. A. O., da Silva, L., Quast, G. R., de la Reza, R., & Jilinski, E. 2000, *AJ*, 120, 1410

Uchida, K. I., et al. 2004, *ApJS*, 154, 439

Walker, H. J., & Wolstencroft, R. D. 1988, *PASP*, 100, 1509

Webb, R. A. 2000a, Ph.D. thesis, UCLA

Webb, R. A., Zuckerman, B., Greaves, J. S., & Holland, W. S. 2000b, *BAAS*, 197, 827

Webb, R. A., Zuckerman, B., Platais, I., Patience, J., White, R. J., Schwartz, M. J., & McCarthy, C. 1999, *ApJ*, 512, L63

Weinberger, A. J., Becklin, E. E., Zuckerman, B., & Song, I. 2004, *AJ*, 127, 2246

Werner, M. W., et al. 2004, *ApJS*, 154, 1

Yin, Q., Jacobsen, S. B., Yamashita, K., Blichert-Toft, J., Télouk, P., & Albarède, F. 2002, *Nature*, 418, 949

Zackarias, N., et al. 2000, *AJ*, 120, 2131

Zackarias, N., Urban, S. E., Zacharias, M. I., Wycoff, G. L., Hall, D. M., Monet, D. G., Rafferty, T. J. 2004, *AJ*, 127, 3043

Zuckerman, B., & Becklin, E. E. 1993, *ApJ*, 414, 793

Zuckerman, B., Webb, R. A., Schwartz, M., & Becklin, E. E. 2001, *ApJ*, 549, L233

TABLE 1
THE TWA SAMPLE

Star ^a	Other Name	Spectral Type	Ref. ^b	distance ^c (pc)	V	Ref. ^d	K_s ^e	T_* ^f (K)
TWA 1	TW Hya	K8e	1	56 ± 7	11.07	1–9	7.30	3700
TWA 2AB	CD–29°8887	M2e+M2	2	...	11.42	1–4,6,8,9	6.71	3500
TWA 3AB	Hen 3-600	M3e+M3.5	2	...	12.04	1,2,6,7	6.77	3300
TWA 4AB	HD 98800	K4+K5	3	47 ± 6	8.89	1–7, 10–15	5.59(A), 5.90(B)	4800(A), 3800(B)
TWA 5A	CD–33°7795	M3e	3	...	11.72	1–5,8,9,16	6.75	3400
TWA 6		K7	4	...	12.00	1–4,6,12,16,17	8.04	4000
TWA 7		M1	4	...	11.06	1–4,6,9,16	6.90	3500
TWA 8A		M2e	4	...	13.30	1–3,6,12	7.43	3300
TWA 8B		M5	4	...			9.01	3100
TWA 9A	CD–36°7429A	K5	4	50 ± 6 ^g	11.32	1–6,9,12	7.85	4200
TWA 9B	CD–36°7429B	M1	4	50 ± 6 ^g	14.10		9.15	3300
TWA 10		M2.5	4	...	12.70	1,2,4,6,12	8.19	3400
TWA 11A	HR 4796A	A0	5	67 ± 2	5.78	2–4,6–9,12	5.77	9250
TWA 12		M2	6	...	13.60	2,4,12,16	8.06	3000
TWA 13A	CD–34°7390A	M1e	1,6	...	12.10	1,4,12,16	7.50	3300
TWA 13B	CD–34°7390B	M1e	1,6	...	12.40		7.46	3200
TWA 14		M0	7	...	13.80	2–4,12,16,18	8.50	3300
TWA 15A		M1.5	7	...	14.10	2,4,16,18	9.68	3500
TWA 15B		M2	7	...	14.00		9.56	3500
TWA 16		M1.5	7	...	12.30	2,4,12,16,18	8.10	3700
TWA 17		K5	7	...	12.70	2,4,5,12,16,18	8.98	4000
TWA 18		M0.5	7	...	12.90	2,4,5,12,16,18	8.84	3800
TWA 19A	HD 102458A	G5	7	104 ± 15	9.10	2–5,7,12,16	7.51	6000
TWA 19B	HD 102458B	K7	7	104 ± 15	11.90	2,4,12,16,18	8.28	4000

^aAB designates binaries that are unresolved by *Spitzer* at $\lambda = 24 \mu\text{m}$.

^bReferences for spectral types and identifications as members of the TWA — (1) Rucinski & Krautter (1983); (2) de la Reza et al. (1989); (3) Gregorio-Hetem et al. (1992); (4) Webb et al. (1999); (5) Houk (1982); (6) Sterzik et al. (1999); (7) Zuckerman et al. (2001).

^cData are from the *Hipparcos Catalog* (Perryman et al. 1997).

^dSources and references for previous optical–IR photometry — (1) Torres et al. (2000); (2) Reid (2003); (3) *Hipparcos-Tycho* (ESA 1997); (4) 2MASS (Cutri et al. 2003); (5) DENIS (Epchtein et al. 1999); (6) Jayawardhana et al. (1999); (7) *IRAS* (Beichman et al. 1988); (8) UCAC1 (Zacharias 2000); (9) Yale-SPM (Platais et al. 1998); (10) Low, Hines, & Schneider (1999); (11) UCAC2 (Zacharias 2004); (12) GSC (Lasker et al. 1990); (13) Soderblom et al. (1998); (14) Prato et al. (2001); (15) Gehrz et al. (1999); (16) Weinberger et al. (2004); (17) USNO A2.0 (Monet 1999); (18) Zuckerman et al. (2001).

^eApparent K_s magnitude is from the 2MASS Point Source Catalog, except for HD 98800, where the K -band magnitudes for both components are from Low, Hines, & Schneider (1999).

^fTemperature of the best-fit Kurucz or NextGen model to the stellar photometry.

^gSee Mamajek, Lawson, & Feigelson (2000) for a discussion of the *Hipparcos* parallax measurement for TWA 9.

TABLE 2
MIPS BANDPASSES

Band	λ_0 (μm)	$\Delta\lambda$ (μm)	scale ($'' \text{ pixel}^{-1}$)	C_ν^a	Phot. Apt. (radius in $''$)	A_ν^b
24 μm	23.7	4.7	2.55	1.042×10^{-3}	15 or 37.5	1.15 or 1.06
70 μm wide field	71	19	9.85	14.9	29.6	1.35
70 μm narrow field	71	19	5.24	52.7	29.7	1.35
160 μm	156	35	16	1.0	64	1.33

^aConversion factor from the calibrated instrumental units of the DAT output to mJy.

^bFactor to correct aperture photometry to that expected from a hypothetical aperture of infinite extent.

TABLE 3
MIPS OBSERVATIONS

Star	Epoch (JD-2453000.0)	24 μm (mJy)	(S/N) _{24 μm}	70 μm^a (mJy)	(S/N) _{70 μm}	160 μm (mJy)	(S/N) _{160 μm}
TW Hya	38.282	2270 ± 230	$> 10^4$	3640 ± 730	170	6570 ± 1310	160
TWA 2AB	35.384	20.1 ± 2.0	200	< 40
Hen 3-600	38.268	1650 ± 170	$> 10^4$	700 ± 140	140	740 ± 190	6
HD 98800AB	177.665	8500 ± 350	1000	6260 ± 1250	200	2100 ± 420	67
TWA 5A	38.255	21.1 ± 2.1	220	< 9
TWA 6	134.825	5.7 ± 0.6	240	< 8
TWA 7	35.398	30.2 ± 3.0	260	85 ± 17	22
TWA 8	35.905	14.5 ± 1.5	160	< 11
A		11.1 ± 1.5					
B		3.4 ± 0.4					
TWA 9	37.870	9.3 ± 1.1	160	< 34
A		6.0 ± 0.6					
B		3.3 ± 0.3					
TWA 10	55.726	5.1 ± 0.5	190	< 8
HR 4796A	35.928	3030 ± 303	$> 10^4$	5160 ± 1100	240	1800 ± 360	55
TWA 12	177.907	5.7 ± 0.6	50	< 29
TWA 13	177.680	17.6 ± 1.8	150	27.6 ± 5.9	13
A		8.8 ± 1.3					
B		8.8 ± 1.3					
TWA 14	55.677	4.1 ± 0.4	27	< 25
TWA 15	55.701	2.9 ± 0.3	72	< 12
A		1.4 ± 0.2					
B		1.5 ± 0.2					
TWA 16	55.714	6.6 ± 0.6	45	< 18
TWA 17	55.743	1.5 ± 0.2	13	< 13
TWA 18	55.762	2.3 ± 0.3	20	< 9
TWA 19A	55.689	10.4 ± 1.1	100	< 27
TWA 19B	55.689	4.6 ± 0.5	44	< 27

^aUpper limits listed are the detected signal within the photometric aperture plus 3σ . If the flux measured within the aperture is less than the background level measured for the aperture, the upper limit listed is 3σ .

TABLE 4
PROPERTIES OF DUST DISKS IN THE TWA

Star	T_{PDS} (K)	R_{PDS} ^a (AU)	M_d (10^{23} g) ^b	L_*/L_\odot ^c	L_{IR}/L_*	L_X/L_*
TW Hya	0.24	2.7×10^{-1}	2.7×10^{-3}
TWA 2AB ^d	< 85	> 7.0	0.27	0.39	< 2.1×10^{-4}	5.9×10^{-4}
Hen 3-600 ^d	0.35	1.2×10^{-1}	6.1×10^{-4}
HD 98800B ^d	160	2.2	> 29 ^e	0.53	2.2×10^{-1}	7.1×10^{-4}
TWA 5A	< 145	> 2.3	0.01	0.36	< 9.6×10^{-5}	1.1×10^{-3}
TWA 6	< 110	> 2.6	0.02	0.14	< 1.4×10^{-4}	1.4×10^{-3}
TWA 7	80	6.8	2.4	0.31	2.0×10^{-3}	7.8×10^{-4}
TWA 8A	< 150	> 1.5	0.04	0.19	< 6.6×10^{-4}	1.3×10^{-3}
TWA 8B	< 70	> 3.2	0.19	0.04	< 7.2×10^{-4}	...
TWA 9A	< 60	> 8.6	1.3	0.15	< 6.8×10^{-4}	1.3×10^{-3}
TWA 9B	< 60	> 4.2	1.5	0.03	< 3.2×10^{-3}	...
TWA 10	< 80	> 3.7	0.09	0.09	< 2.6×10^{-4}	1.1×10^{-3}
HR 4796A	108	30	110	19.7	4.8×10^{-3}	...
TWA 12	< 65	> 6.0	0.94	0.09	< 1.0×10^{-3}	1.0×10^{-3}
TWA 13A	65	7.8	1.4	0.18	8.6×10^{-4}	1.8×10^{-3}
TWA 13B	65	7.7	1.4	0.17	8.9×10^{-4}	...
TWA 14	< 65	> 5.1	0.59	0.07	< 8.8×10^{-4}	1.4×10^{-3}
TWA 15A	< 60	> 3.5	0.27	0.03	< 8.2×10^{-4}	4.7×10^{-3}
TWA 15B	< 65	> 3.1	0.20	0.03	< 7.9×10^{-4}	...
TWA 16	< 80	> 4.5	0.15	0.12	< 2.8×10^{-4}	7.0×10^{-4}
TWA 17	< 60	> 5.1	0.54	0.06	< 7.8×10^{-4}	9.8×10^{-4}
TWA 18	< 80	> 3.1	0.06	0.06	< 2.6×10^{-4}	9.8×10^{-4}
TWA 19A	< 95	> 13	1.0	2.10	< 2.2×10^{-4}	7.1×10^{-4}
TWA 19B	< 70	> 11	2.7	0.38	< 8.2×10^{-4}	...

^aThe minimum distance from a star for dust in thermal equilibrium at temperature, T_{PDS} , is given by $R_{PDS} = 0.5(T_*/T_{PDS})^2 R_*$, where R_* is radius of the star.

^bThe estimated minimum mass in dust, M_d , consistent with the observations for systems where T_{PDS} can be determined or constrained, and assuming that the circumstellar debris is optically thin. An average dust grain size of $2.8 \mu\text{m}$ in radius and a density for the material of $\rho = 2.5 \text{ g cm}^{-3}$ are assumed (Chen & Jura 2001). For systems with no detected IR excesses, M_d is an estimate using the limits determined for R_{PDS} and L_{IR}/L_* .

^cA distance to the TWA of 55 pc is assumed except for the five systems with measured parallaxes. For these systems, the distances listed in Table 1 are used to determine L_* .

^dTWA 2, Hen 3-600, and HD 98800B are binaries and both stellar components are included in the luminosity values.

^eThe minimum dust mass for the HD 98800B debris system is likely to be underestimated because the assumption that the circumstellar material is optically thin in the IR is not valid (see, Low, Hines, & Schneider 1999).

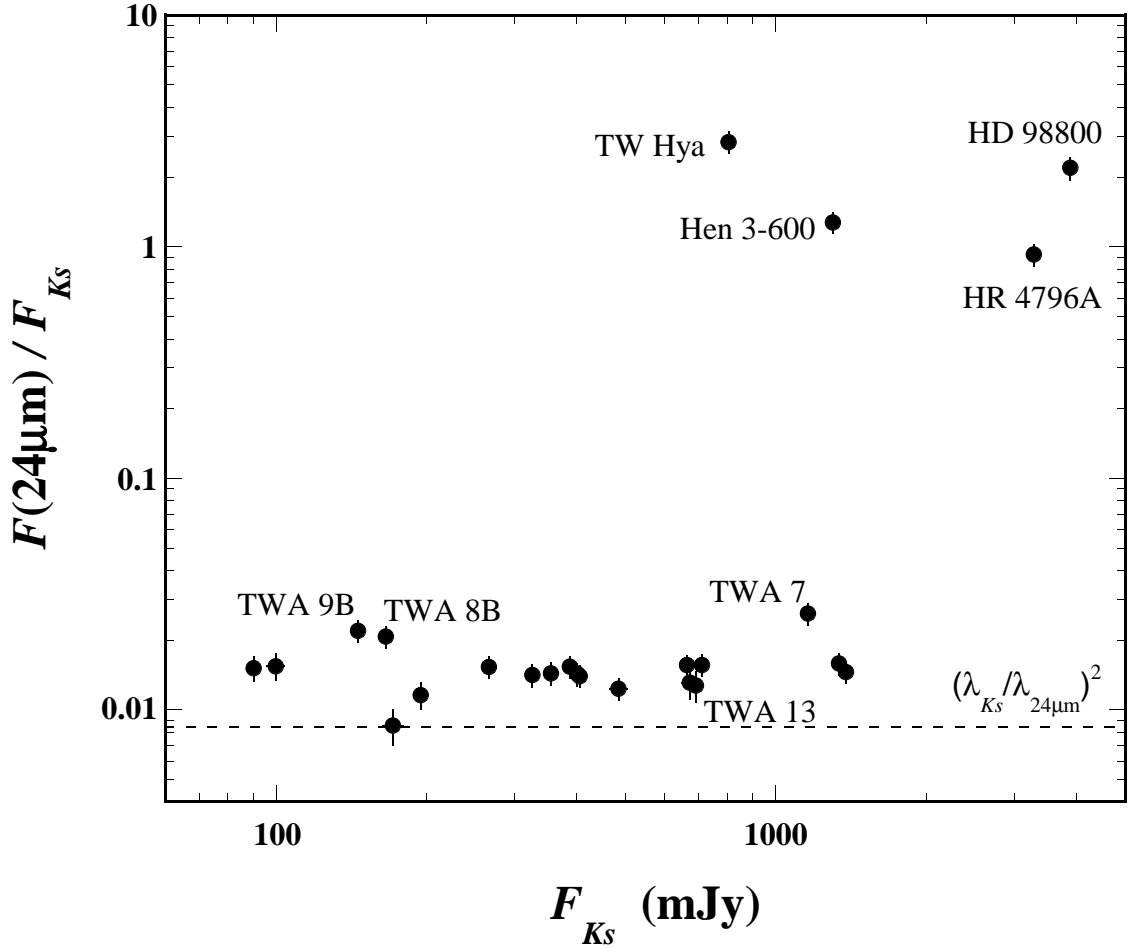


FIG. 1.— MIPS 24 μ m photometry compared to the 2MASS K_s -band measurements of the TWA sample. The dashed line represents the $F_{24\mu\text{m}}$ -to- F_{Ks} ratio under the assumption that both photometric bands lie on the Rayleigh-Jeans tail of the stellar spectrum.

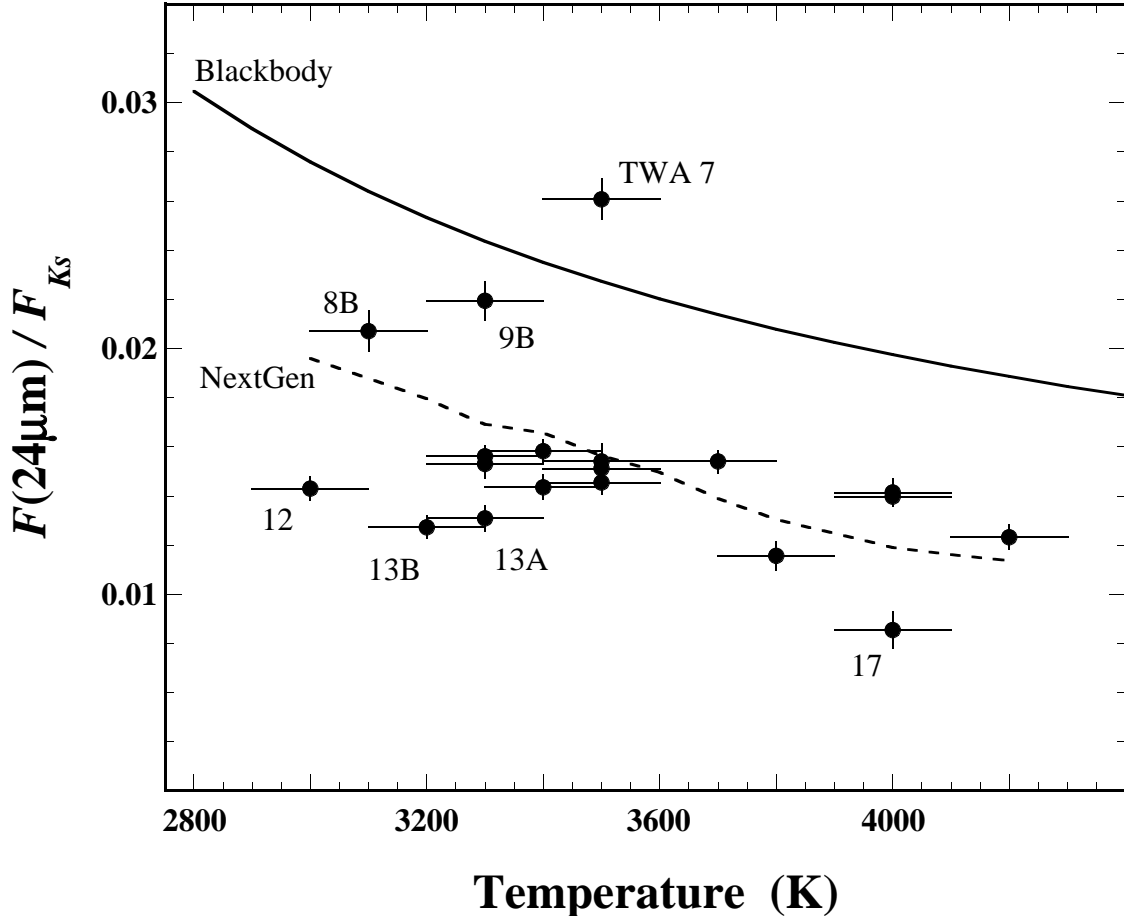


FIG. 2.— The ratio of the observed 24 μm flux density to that determined for the K_s -band from the 2MASS Point Source Catalog plotted against the best-fitting model temperature of the stars. TW Hya, Hen 3-600, HD 98800, HR 4796A, and TWA 19A are not shown so that TWA members with $T < 6000\text{K}$ or without a large 24 μm excess can be displayed in more detail. The *solid* curve represents the flux ratio between the two filter bandpasses for a blackbody. Likewise, the *dashed* curve is the ratio determined from the NextGen models used to estimate the 24 μm and 70 μm photospheric flux densities.

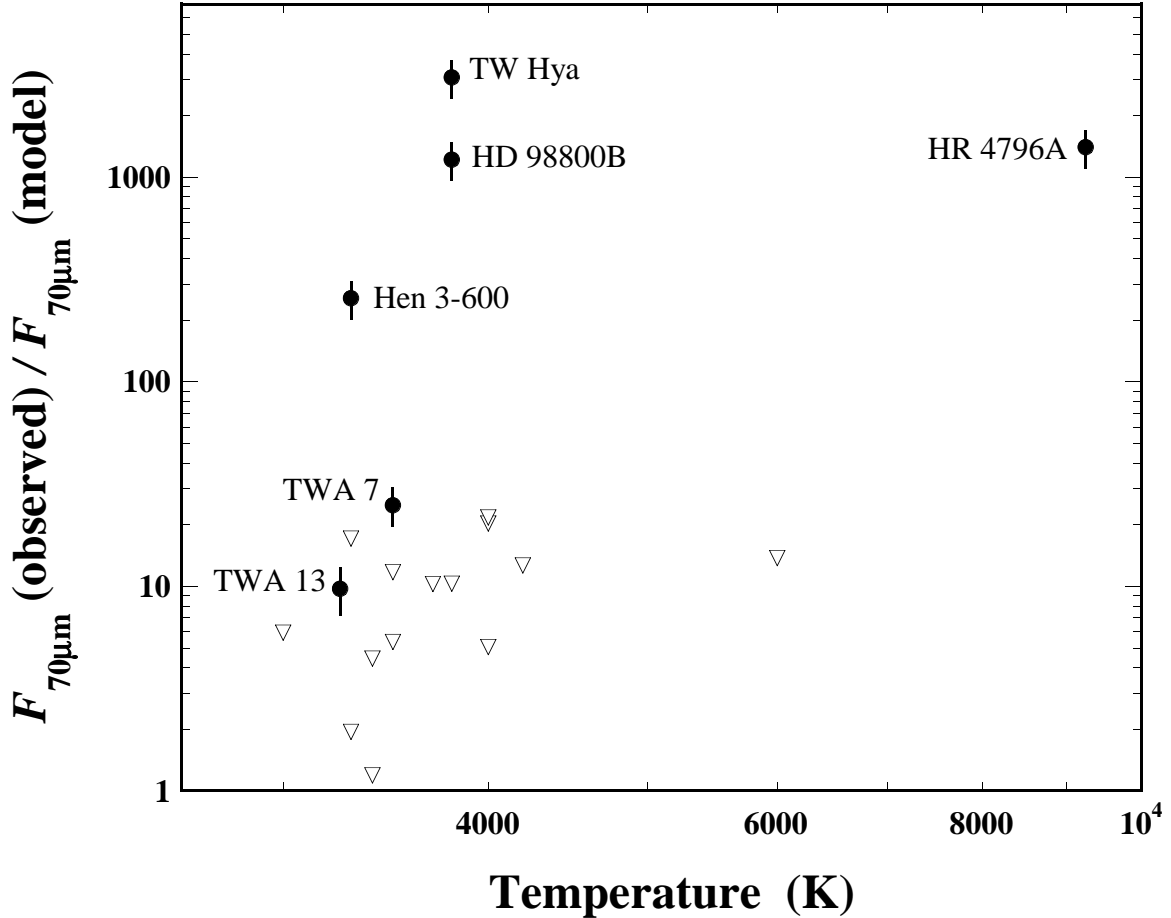


FIG. 3.— The $70\text{ }\mu\text{m}$ excesses measured by *Spitzer* relative to the predicted $70\text{ }\mu\text{m}$ flux densities of the stars in the TWA. As in Figure 2, the data are plotted against the model temperature of the stellar photospheres. Each star detected by MIPS at $70\text{ }\mu\text{m}$ is labeled. One-sigma upper limits are denoted by *open triangles*.

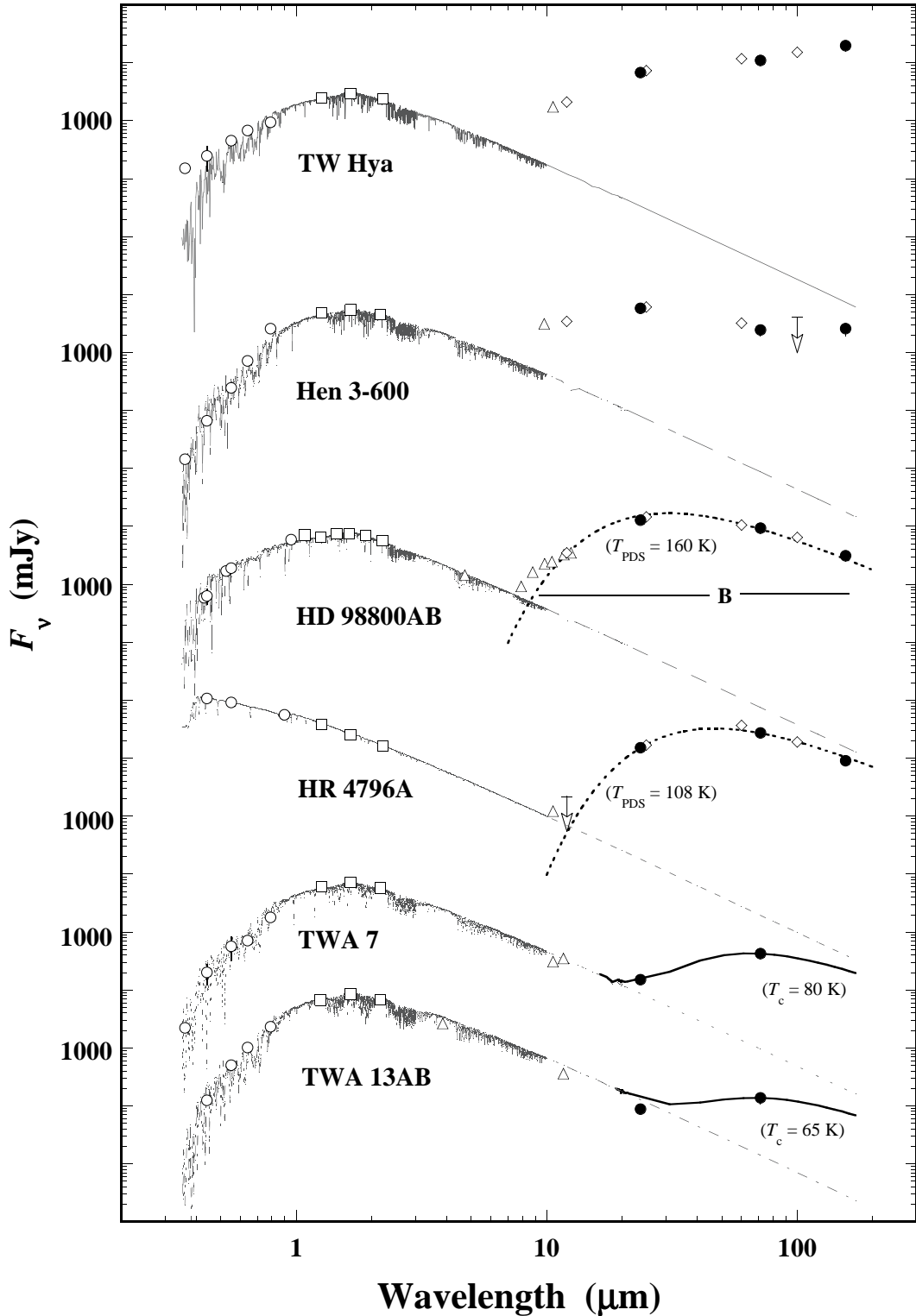


FIG. 4.— The SEDs of the six TWA members with confirmed IR excesses. Model stellar photospheres are shown for the stars, along with available photometric measurements from 0.36–160 μm . Measurements made by MIPS are denoted by *filled circles*. Data from the literature are shown by *open symbols*. References to the optical (*circles*), near-IR (*squares*), ground-based mid-IR (*triangles*), and *IRAS* (*diamonds* and upper limits) photometry are given in Table 1. Gehrz et al. (1999) showed that HD 98800B produces the IR excess in this binary system, though the sum of the models and observed flux densities of A and B are plotted. Blackbody fits to the MIPS and *IRAS* data for HD 98800B and HR 4796A are shown as bold *dashed* curves. The bold *solid* curves shown for TWA 7 and 13AB are the sum of the photospheres and IR excesses assuming that the excesses are described by blackbodies having $T_{PDS} = 60$ –80 K. Color temperatures (T_c) for TWA 7 and 13AB are also displayed. The SEDs have been spaced apart for clarity and a 1000 mJy fiducial is labeled for each star. To recover the measured flux densities in mJy, multiply the SEDs by the following factors: 0.33 (TW Hya), 0.29 (Hen 3-600), 0.67 (HD 98800AB), and 0.2 (HR 4796A, TWA 7, and 13AB).

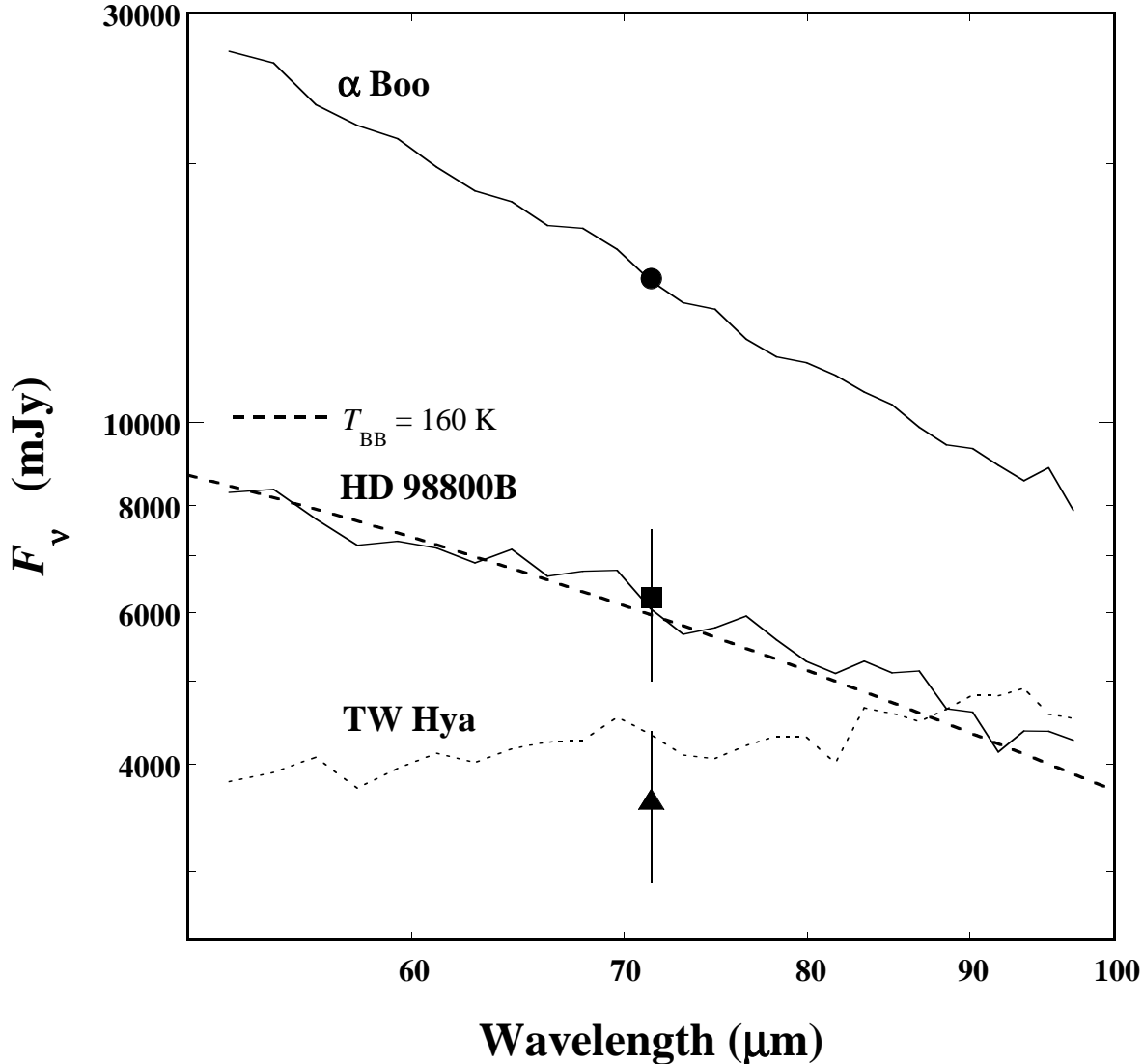


FIG. 5.— MIPS SED-mode spectra of TW Hya and HD 98800B. For comparison, the spectrum of α Boo is displayed and was used to calibrate the fluxes and spectral shapes of the two TWA members. The broad-band flux densities measured from the MIPS 70 μm photometry are shown for TW Hya (square) and HD 98800B (triangle). The spectra are calibrated assuming that $F_\nu = 14.7$ Jy at the effective wavelength of the 70 μm bandpass for α Boo (circle), and that its spectrum is adequately described at these wavelengths by $F_\nu \propto \nu^2$. The best-fit blackbody to the IR excess of HD 98800B using the broad-band infrared measurements from IRAS, Spitzer-MIPS, and the ground is shown by the dashed curve and has a temperature, $T_{\text{BB}} = 160$ K (see Figure 4). Most of the apparent “noise” in the SED-mode spectra is caused by pixel-to-pixel sensitivity variations of the 70 μm array.